Quantum Study of the Absorption Spectroscopy of Bis(triarylamine) Radical Cations

J. Seibt,[†] A. Schaumlöffel,[†] C. Lambert,[‡] and V. Engel*,[†]

Institut für Physikalische Chemie, Universität Würzburg, Am Hubland, D-97074 Würzburg, Germany, and Institut für Organische Chemie, Universität Würzburg, Am Hubland, D-97074 Würzburg, Germany

Received: May 30, 2008; Revised Manuscript Received: July 23, 2008

Absorption spectra of bridged triarylamine radical cations are calculated quantum mechanically which extends our previous classical analysis (Lambert et al. *J. Phys. Chem. A* **2004**, *108*, 6474). A comparison between spectra determined within a diabatic and an adiabatic representation shows that under certain circumstances deviations occur. It is found that the latter are mainly caused by the Condon approximation for the dipole moments. The inclusion of vibrational degrees of freedom leads to an excellent agreement with experiment.

1. Introduction

While electron and hole transfer processes play an important role in many physical, chemical, and biochemical processes,[1−4] it is often advantageous to look at simple model systems in order to investigate basic charge transfer aspects. For this purpose, mixed valence (MV) compounds have often been employed.[5−8] In these compounds, at least two redox centers with different redox states are connected by a bridge unit. These redox centers may be metal complexes or purely organic redox active groups[9] while the bridge may be saturated or unsaturated.[10,11] It is the goal of this paper to describe the optical transitions in organic MV compounds quantum mechanically within a three-state model which involves the states localized at the redox centers and, as a third state, the bridge.[12−17]

Recently, we investigated a series of organic bis(triarylamine) radical cation MV compounds $\mathbf{1}^+$−$\mathbf{3}^+$ in which the triarylamine redox centers are connected by different unsaturated bridges, though the N−N distance was kept fixed.[13] The structures of the three compounds are shown in Figure 1. In methylene chloride solution, the radical cations $\mathbf{1}^+$ and $\mathbf{2}^+$ display three distinct absorption features in the near-infrared region (NIR): a sharp band at ca. 13000 cm $^{-1}$ which is due to a localized $\pi-\pi^*$ excitation in the triarylamine radical cation moiety,[18] a band (shoulder) at 11000 cm $^{-1}$ which is due to an optically induced hole transfer from the triarylamine radical cation to the bridge, and, a third very broad band at ca. 6000−8000 cm^{-1} which is associated with the optically induced hole transfer form one triarylamine to the other. The latter band is usually called intervalence charge transfer (IV-CT) band. For $\mathbf{3}^+$ the situation is much different: at 12500 cm^{-1} a band typical of localized anthracene radical cations is observed and at ca. 5000 cm^{-1} a band that is associated with the transfer of a hole from the anthracene to either triarylamine.

The electronic states that are involved in the above-mentioned transitions can be modeled by applying a three-state approximation in which three diabatic (formally noninteracting) states are mixed, see ref 13. These are the ones where the positive charge is localized either at triarylamine or at the bridge. While the former states are degenerate in energy, the latter one is higher in energy for $\mathbf{1}^+$ and $\mathbf{2}^+$ by the free energy difference $\Delta G°$ but is lower in energy for $\mathbf{3}^+$ (see below). These three diabatic states may be coupled in a 3 × 3 Hamilton matrix via electronic couplings V_{ij} to yield, upon diagonalization, three adiabatic states. For $\mathbf{1}^+$ and $\mathbf{2}^+$ this yields a double minimum (adiabatic) potential surface for the ground state but a single minimum potential for $\mathbf{3}^+$; that is, in $\mathbf{1}^+$ and $\mathbf{2}^+$ the hole is localized at one triarylamine group whereas in $\mathbf{3}^+$ the hole is localized at the anthracene bridge. If one assumes harmonic potentials for each diabatic state, one can construct potential energy surfaces in two dimensions using an asymmetric ET (electron transfer) coordinate x and a symmetric ET coordinate y. Intuitively it is easy to understand why at least one (averaged) asymmetric and one symmetric mode is necessary for a three-state model: The asymmetric mode x transforms one asymmetric (symmetry broken) state into its degenerate mirror image. This process

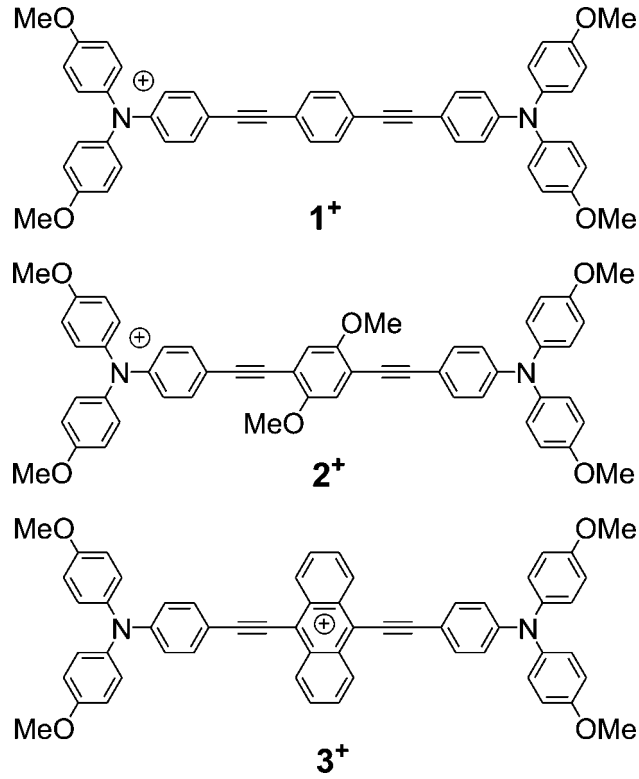

Figure 1. Structure of the three mixed valence compounds where the triarylamine redox centers are connected by different bridge units.

* Corresponding author: Phone, +49-931-888-6376; Fax, +49-931-888-6362; E-mail, voen@phys-chemie.uni-wuerzburg.de.
† Institut für Physikalische Chemie.
‡ Institut für Organische Chemie.

10.1021/jp804779s CCC: $40.75
Published on Web 09/24/2008

proceeds via a symmetrical transition state. The symmetric mode y transforms this symmetric transition state into the symmetric state in which the charge is localized at the bridge. The minima of the diabatic potential surfaces are chosen in a way that the dimensionless distance between each minimum is unity.[13]

The hole transfer processes between different adiabatic states are governed mainly by three parameters, the electronic coupling, the free energy difference $\Delta G°$, and the reorganization energies associated with the potential curvature of the diabatic states. Applying Marcus−Hush (MH) theory[19,20] and the generalized Mulliken−Hush (GMH) theory,[21−23] we were able to deduce the electronic coupling and the reorganization parameters by analysis of the absorption bands associated with transitions between the adiabatic states. The Mulliken−Hush theory rests on the assumption of Boltzmann distributed ground states with infinitely small vibronic level spacings at the high-temperature limit. A classical calculation of energy differences to the excited-state surfaces then yields the electronic transitions as (in the two-level approximation) Gaussian-shaped bands. This theory however neglects discrete vibronic effects. Recent work by Hupp et al.,[24,25] Zink et al.,[26,27] and by us[28] devoted to the description of vibronic effects within a two-state model. Because in systems with a low-lying bridge state it might be advantageous to include this second excited state in the treatment, it is the goal of this work to present a quantum mechanical formulation within a three-level approach which will yield more precise information about the connection of vibronic modes and reorganization parameters that are involved in the IV-CT transitions.

The paper is organized as follows: in section 2, the theoretical methods and the model employed to calculated the spectra are summarized. The results and a comparison between theory and experiment are presented in section 3. Finally, a summary in section 4 concludes the present article.

2. Theory and Model

2.1. Generalized Mulliken−Hush Theory. We start with an outline of the method usually employed to describe the optical properties of IV-CT systems. The Hamiltonians for the bis(triarylamine) cations are constructed following the generalized Mulliken−Hush theory.[21−23] Details of this procedure are given in ref 13, and we here only summarize the key steps. The starting point is an adiabatic (*a*) representation of the three state Hamiltonian which reads

$$\mathbf{H}_{\mathrm{GMH}}{}^{\mathrm{a}} = \begin{pmatrix} V_1{}^{\mathrm{a}} & 0 & 0 \\ 0 & V_2{}^{\mathrm{a}} & 0 \\ 0 & 0 & V_3{}^{\mathrm{a}} \end{pmatrix} - E \begin{pmatrix} \mu_{11}{}^{\mathrm{a}} & \mu_{12}{}^{\mathrm{a}} & \mu_{13}{}^{\mathrm{a}} \\ \mu_{21}{}^{\mathrm{a}} & \mu_{22}{}^{\mathrm{a}} & \mu_{23}{}^{\mathrm{a}} \\ \mu_{31}{}^{\mathrm{a}} & \mu_{32}{}^{\mathrm{a}} & \mu_{33}{}^{\mathrm{a}} \end{pmatrix} \quad (1)$$

where the $V_n{}^{\mathrm{a}}$ are transition energies usually taken as the absorption band positions determined from experiment. The second term describes an electric dipole interaction which contains the matrix elements of the projection of the dipole operator on the field polarization vector, and E is the electric field. The dipole matrix elements are assumed to be independent of the nuclear coordinates (Condon approximation). We note that, because we deal with ionic systems where the dipole operator is not translational invariant, it is advantageous to work with the differences $\mu_{nn}{}^{\mathrm{a}} - \mu_{11}{}^{\mathrm{a}}$,[13] which amounts to a shift in the eigenvalues of the Hamiltonian $H_{\mathrm{GMH}}{}^{\mathrm{a}}$. Performing a unitary transformation with a matrix **C** diagonalizing the dipole matrix, one arrives at the (diabatic (d)) Hamiltonian

$$\mathbf{H}_{\mathrm{GMH}}{}^{\mathrm{d}} = \mathbf{C}^{\mathrm{t}}\mathbf{H}_{\mathrm{GMH}}{}^{\mathrm{a}}\mathbf{C} = \begin{pmatrix} V_{11}{}^{\mathrm{d}} & V_{12}{}^{\mathrm{d}} & V_{13}{}^{\mathrm{d}} \\ V_{21}{}^{\mathrm{d}} & V_{22}{}^{\mathrm{d}} & V_{23}{}^{\mathrm{d}} \\ V_{31}{}^{\mathrm{d}} & V_{32}{}^{\mathrm{d}} & V_{33}{}^{\mathrm{d}} \end{pmatrix} - E \begin{pmatrix} \mu_{11}{}^{\mathrm{d}} & 0 & 0 \\ 0 & \mu_{22}{}^{\mathrm{d}} & 0 \\ 0 & 0 & \mu_{33}{}^{\mathrm{d}} \end{pmatrix} \quad (2)$$

where $V_{13}{}^{\mathrm{d}} = V_{31}{}^{\mathrm{d}}$, $V_{12}{}^{\mathrm{d}} = V_{21}{}^{\mathrm{d}}$, and $V_{23}{}^{\mathrm{d}} = V_{32}{}^{\mathrm{d}}$, due to symmetry. As outlined in ref 13, we employ two values for the coupling so that the respective diabatic potential matrix is

$$\begin{pmatrix} V_{11}{}^{\mathrm{d}} & V_{\mathrm{BR}}{}^{\mathrm{d}} & V_{\mathrm{IV}}{}^{\mathrm{d}} \\ V_{\mathrm{BR}}{}^{\mathrm{d}} & V_{22}{}^{\mathrm{d}} & V_{\mathrm{BR}}{}^{\mathrm{d}} \\ V_{\mathrm{IV}}{}^{\mathrm{d}} & V_{\mathrm{BR}}{}^{\mathrm{d}} & V_{33}{}^{\mathrm{d}} \end{pmatrix} \quad (3)$$

Thus, with knowledge of the transition energies $V_n{}^{\mathrm{a}}$ and the adiabatic dipole matrix elements it is possible to derive the diabatic coupling matrix in eq 2 which serves as a starting point for a further parametrization.

In the construction of the Hamiltonian, the constant diagonal elements $V_{nn}{}^{\mathrm{d}}$ of $\mathbf{H}_{\mathrm{GMH}}{}^{\mathrm{d}}$ are replaced by potential surfaces depending on two effective, dimensionless coordinates (x, y) along which the charge transfer occurs. The following form is obtained

$$V_{11}{}^{\mathrm{d}}(x,y) = \lambda_1 \left[\frac{\left(x+\frac{1}{2}\right)^2 + C\left(x+\frac{1}{2}\right)^4 + y^2 + Cy^4}{1+C} \right] \quad (4)$$

$$V_{22}{}^{\mathrm{d}}(x,y) = \lambda_2 \left[x^2 + \left(\frac{\sqrt{3}}{2} - y\right)^2 \right] + \Delta G° \quad (5)$$

$$V_{33}{}^{\mathrm{d}}(x,y) = \lambda_3 \left[\frac{\left(x-\frac{1}{2}\right)^2 + C\left(x-\frac{1}{2}\right)^4 + y^2 + Cy^4}{1+C} \right] \quad (6)$$

In these equations, $\lambda_1 = \lambda_3$ is the total (=vibrational + solvent) reorganization energy of the triarylamine localized states and λ_2 is the reorganization energy associated with the bridge localized state. The parameter C augments the diabatic harmonic potentials by a quartic term which was necessary to adjust the calculated bandwidth to the experiment in the classical analysis given in ref 13. The energy $\Delta G°$ displaces the bridge state vertically. The topology of the potential surfaces is illustrated for the $\mathbf{1}^+$ system in Figures 2 and 3. The diabatic surfaces (Figure 2) exhibit the two minima for the triarylamine localized states at $x = \pm 0.5$ and $y = 0$ (panels a and c), whereas the minimum of the bridge localized potential (panel b) occurs at the $x = 0$ position but is shifted along the symmetric coordinate y. Switching to the adiabatic representation yields nonintersecting surfaces (Figure 3) with a double minimum topology in the ground state and single minima in the excited states.

The reorganization parameters for the three system n^+ (n = **1**, **2**, **3**) are summarized in Table 1 which also contains electronic couplings and the dipole matrix elements. The detailed way in which these quantities were determined is given in ref 13; here, the procedure is outlined only briefly: The adiabatic transition moments and the transition energies were determined experimentally from the absorption spectra. The adiabatic dipole moment differences were computed by quantum chemical methods as these quantities are not accessible experimentally. We employed the AM1-CI method to obtain

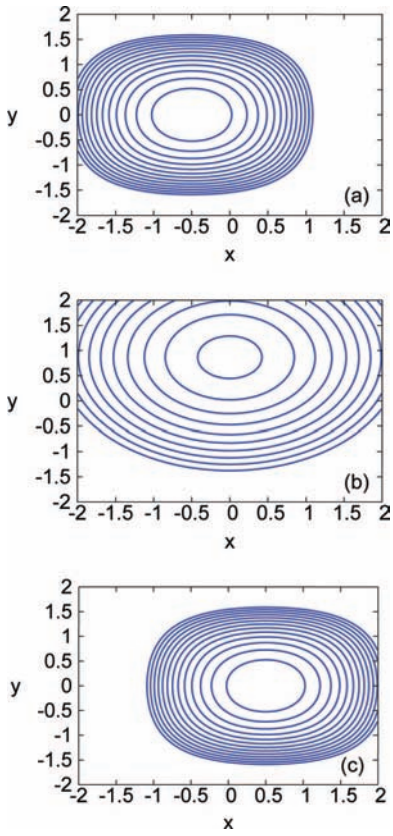

Figure 2. Diabatic potential energy surfaces of the $\mathbf{1}^+$ system. Panels a and c correspond to the two triarylamine localized states whereas the bridge potential is shown in panel b. Contours are shown starting at a value of 2000 cm^{-1} and increasing in steps of 2000 cm^{-1}.

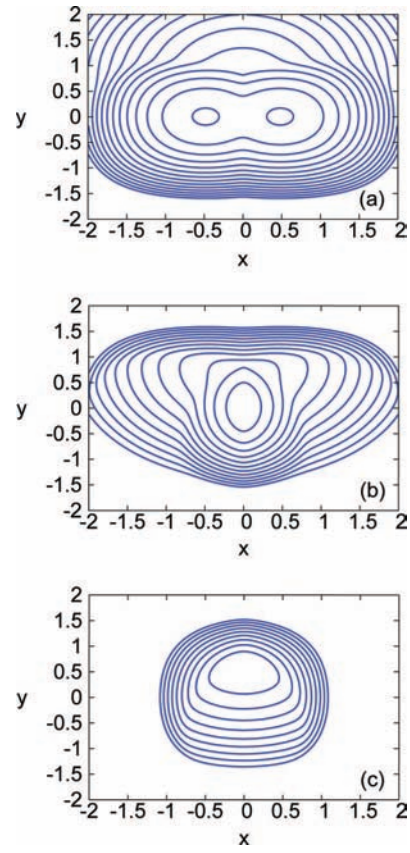

Figure 3. Adiabatic potential energy surfaces of $\mathbf{1}^+$ for the ground (panel a), first (panel b), and second excited state (c). Contours are shown starting at a value of 2000 cm^{-1} and increasing in steps of 2000 cm^{-1}.

the dipole moments. The validity of this approach is discussed in detail in ref 13. Then we derived all diabatic quantities from the adiabatic values by GMH theory. The diabatic electronic couplings together with eqs 6 were then used to calculate the potential energy surfaces. We used these potential energy surfaces to calculate the absorption spectra in a classical way (see Introduction). The reorganization parameters were then determined by a best fit of the derived absorption spectra to the experimental spectra.

2.2. Hamiltonians for the Quantum Propagation. In our quantum calculation, two representations of the Hamiltonian are employed. The diabatic Hamiltonian $\mathbf{H}^d$ consists of the sum of the GMH Hamiltonian eq 2 including the kinetic energy operators and the potential surfaces $V_{nn}^d(x,y)$

$$\mathbf{H}^d = \begin{pmatrix} T & 0 & 0 \\ 0 & T & 0 \\ 0 & 0 & T \end{pmatrix} + \begin{pmatrix} V_{11}^d(x,y) & V_{BR} & V_{IV} \\ V_{BR} & V_{22}^d(x,y) & V_{BR} \\ V_{IV} & V_{BR} & V_{33}^d(x,y) \end{pmatrix} - E \begin{pmatrix} \mu_{11}^d & 0 & 0 \\ 0 & \mu_{22}^d & 0 \\ 0 & 0 & \mu_{33}^d \end{pmatrix} \quad (7)$$

Here, T denotes the kinetic energy operator for the nuclear degrees of freedom

$$T = -\frac{1}{2m}\frac{\partial^2}{\partial x^2} - \frac{1}{2m}\frac{\partial^2}{\partial y^2} \quad (8)$$

Note that, because dimensionless coordinates are employed, the mass parameter has the unit of an inverse energy. The values of the mass are given in units of eV^{-1} throughout without repeating this explicitely. In order to keep the number of parameters small, we choose the mass to be the same for the two vibrational degrees of freedom. This, in general, will have to be modified.

We now switch to the adiabatic representation by performing a unitary transformation of the Hamiltonian $\mathbf{H}^d$. The coordinate-dependent transformation matrix $\mathbf{A}(x,y)$ is defined as the one which diagonalizes the diabatic potential matrix. In more detail, we have

$$\mathbf{H}^a = \mathbf{A}\mathbf{H}^d\mathbf{A}^t = \mathbf{A}\begin{pmatrix} T & 0 & 0 \\ 0 & T & 0 \\ 0 & 0 & T \end{pmatrix}\mathbf{A}^t + \begin{pmatrix} V_1^a(x,y) & 0 & 0 \\ 0 & V_2^a(x,y) & 0 \\ 0 & 0 & V_3^a(x,y) \end{pmatrix} - E\mathbf{A}\begin{pmatrix} \mu_{11}^d & 0 & 0 \\ 0 & \mu_{22}^d & 0 \\ 0 & 0 & \mu_{33}^d \end{pmatrix}\mathbf{A}^t \quad (9)$$

The transformation of the matrix containing the kinetic energy operators introduces kinetic coupling elements which, in what follows, are ignored. Furthermore, a coordinate dependence is introduced in the adiabatic dipole-matrix elements. This dependence is neglected in our treatment, i.e., the dipole matrix is taken as the one constructed from GMH theory (see eq 1) so that the adiabatic Hamiltonian is

$$\mathbf{H}^{a} = \begin{pmatrix} T & 0 & 0 \\ 0 & T & 0 \\ 0 & 0 & T \end{pmatrix} + \begin{pmatrix} V_1^{a}(x,y) & 0 & 0 \\ 0 & V_2^{a}(x,y) & 0 \\ 0 & 0 & V_3^{a}(x,y) \end{pmatrix} - E \begin{pmatrix} \mu_{11}^{a} & \mu_{12}^{a} & \mu_{13}^{a} \\ \mu_{21}^{a} & \mu_{22}^{a} & \mu_{23}^{a} \\ \mu_{31}^{a} & \mu_{32}^{a} & \mu_{33}^{a} \end{pmatrix} \quad (10)$$

where now the molecular Hamiltonian is diagonal and the interaction term carries an off-diagonal coupling. The Hamiltonians in the adiabatic ($\mathbf{H}^{a}$) and diabatic ($\mathbf{H}^{d}$) representation are the basis for the calculation of absorption spectra as discussed below.

It has to be kept in mind that, within the GMH theory, the adiabatic and diabatic Hamiltonians are equivalent because they are connected by a unitary transformation. The introduction of a coordinate-dependent unitary transformation, on the other hand, introduces a coordinate dependence in the adiabatic dipole matrix and also gives rise to kinetic coupling terms. The approximations leading to the adiabatic Hamitonian in eq 10 mean that the here adopted two representations are not equivalent and one or the other might be more convenient to describe spectroscopic properties of the molecules under consideration. Below we show that that the adiabatic representation offers a simple approach to model and interpret the absorption spectra of the here treated bis(triarylamine) radical cations.

2.3. Absorption Spectra. Absorption spectra are calculated adopting the time-dependent approach to spectroscopy.[29−32] Starting from an initial state $|\psi_i>$ with energy E_i, the spectrum is given as (atomic units are employed)

$$\sigma_i(E_{ph}) \sim \int_{-\infty}^{\infty} dt\ e^{-i(E_i+E_{ph})t} c_i(t) w(t) \quad (11)$$

where E_{ph} denotes the photon energy. The spectrum appears as the Fourier transform of a time-correlation function defined as

$$c_i(t) = \langle \mu\psi_i | e^{-iHt} | \mu\psi_i \rangle \quad (12)$$

were μ is the projection of the dipole operator on the electric field polarization vector. Calculation of the correlation function involves evaluation of the overlap between the initial state (times the dipole operator) and its time-propagated state. In eq 11, a window function $w(t)$ is introduced which damps the correlation function for longer times. In this way we phenomenologically account for the influence of an environment leading to a line broadening.[33] The numerically given energy resolutions in section 3 are calculated as $\Delta E_{res} = \hbar 8\ \ln(2)/\Delta_t$, which gives the relation between the width (full width at half-maximum) of a Gaussian in energy (ΔE_{res}) and time (Δ_t) domain.

We now modify the general expression for the correlation function according to our purposes. A similar approach has been applied before to characterize absorption and emission properties of molecules with excited-state mixed valence states within a two-state model.[34]In the adiabatic approach the calculation of spectra for transitions from the ground state $|1>$ to the higher states $|2>$ and $|3>$ separates. The initial state is defined as the system's ground state of energy E_i^{a} defined by

$$(T + V_1^{a}(x,y))\ \ \psi_{1,i}^{a}(x,y) = E_i^{a}\ \ \psi_{1,i}^{a}(x,y) \quad (13)$$

The correlation functions then are obtained as

$$C_{in}^{a} = \langle \mu_{1n}^{a}\ \ \psi_{1,i}^{a}(x,y) | e^{-iH_n^{a}t} \mu_{1n}^{a}\ \ \psi_{1,i}^{a}(x,y) \rangle \quad (14)$$

where the brackets denote integration over the nuclear degrees of freedom (x, y). The total spectrum is then obtained as the sum

$$\sigma_i^{a}(E_{ph}) \sim \sum_n \sigma_{in}^{a}(E_{ph}) = \sum_n \int_{-\infty}^{\infty} dt\ \ e^{-i(E_i+E_{ph})t} c_{in}^{a}(t) \quad (15)$$

where the index (n) runs over all excited states with nonvanishing transition dipole moment. The time evolution is obtained with the propagator containing the adiabatic Hamiltonian in state $|n>$, $H_n^{a} = T + V_n^{a}(x,y)$.

In the diabatic representation, the initial state $\underline{\psi}_i^{d}$ has three components and fulfills the time-independent Schrödinger equation

$$\mathbf{H}_0^{d} \begin{pmatrix} \psi_{1,i}^{d} \\ \psi_{2,i}^{d} \\ \psi_{3,i}^{d} \end{pmatrix} = E_i^{d} \begin{pmatrix} \psi_{1,i}^{d} \\ \psi_{2,i}^{d} \\ \psi_{3,i}^{d} \end{pmatrix} \quad (16)$$

where we have not explicitely distinguished between a vector and its transposed, and $\mathbf{H}_0^{d}$ is the molecular part of the total Hamiltonian given in eq 7. According to the three-component wave function there is a single correlation function to be determined as

$$c_i^{d} = \langle \underline{\varphi}^{d} | e^{-i\mathbf{H}_0^{d}t} \underline{\varphi}^{d} \rangle = \left\langle \begin{pmatrix} \mu_1^{d}\psi_{1,i}^{d} \\ \mu_2^{d}\psi_{2,i}^{d} \\ \mu_3^{d}\psi_{3,i}^{d} \end{pmatrix} | e^{-i\mathbf{H}_0^{d}t} \begin{pmatrix} \mu_1^{d}\psi_{1,i}^{d} \\ \mu_2^{d}\psi_{2,i}^{d} \\ \mu_3^{d}\psi_{3,i}^{d} \end{pmatrix} \right\rangle \quad (17)$$

The spectrum for transitions into all states (σ_i^{d}) is obtained by a single Fourier transform of this function. The problem here is that this formalism includes a transition from the initial (ground) state into itself and the spectrum exhibits a large intensity peak around the ground-state energy. This, of course, does not make much sense, and therefore, the state $\underline{\varphi}^{d}$ at time $t = 0$ is replaced as

$$\underline{\varphi}^{d} \rightarrow \underline{\varphi}^{d} - \langle \underline{\psi}_i^{d} | \underline{\varphi}^{d} \rangle\ \underline{\psi}_i^{d} \quad (18)$$

i.e., we project out the contribution from the initial wave function. All propagations are performed with the split-operator method by Feit and Fleck[35] adapted to the case where the Hamiltonian is a matrix.[36] The stationary states are obtained by imaginary time propagation.[37]

3. Results

We start with the calculation of the absorption spectra in the approximation that the kinetic energy operators are negligible which corresponds to the limiting case of an infinite mass m.

TABLE 1: Model Parameters Employed in the Construction of the Potential Energy Surfaces

system	1^+	2^+	3^+
λ_1 (cm^{-1})	8500	7400	3000
λ_2 (cm^{-1})	3800	9200	3000
ΔG° (cm^{-1})	7600	900	−1900
V_{BR}^{d} (cm^{-1})	1070	1270	1660
V_{IV}^{d} (cm^{-1})	1000	1910	430
C	0.2	0.0	0.0
μ_{12}^{a} (D)	6.2	9.7	14.1
μ_{13}^{a} (D)	4.7	6.8	0.0
μ_{11}^{d} (D)	71.6	46.7	36.0
μ_{22}^{d} (D)	−0.9	−3.0	0.0
μ_{33}^{d} (D)	36.0	6.1	−36.0

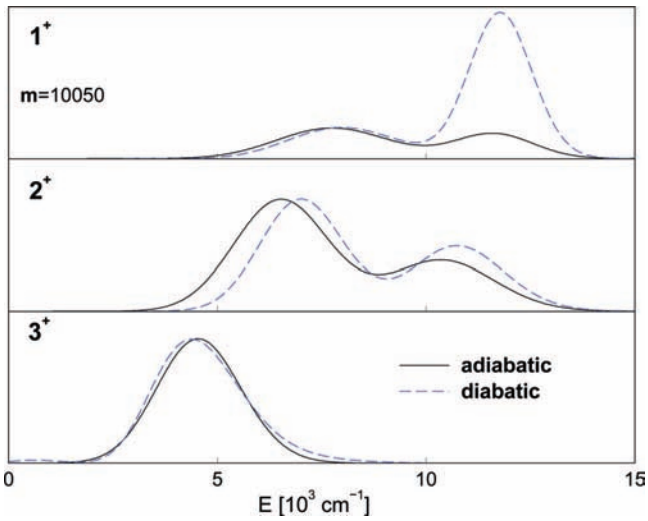

Figure 4. Comparison of absorption spectra calculated employing an adiabatic and a diabatic representation. Spectra are shown for a mass parameter of $m = 10050$ eV^{-1} and for the three compounds $\mathbf{n}^+$, as indicated. The adiabatic/diabatic curves are normalized to have the same maximum height at their respective low energy extremum.

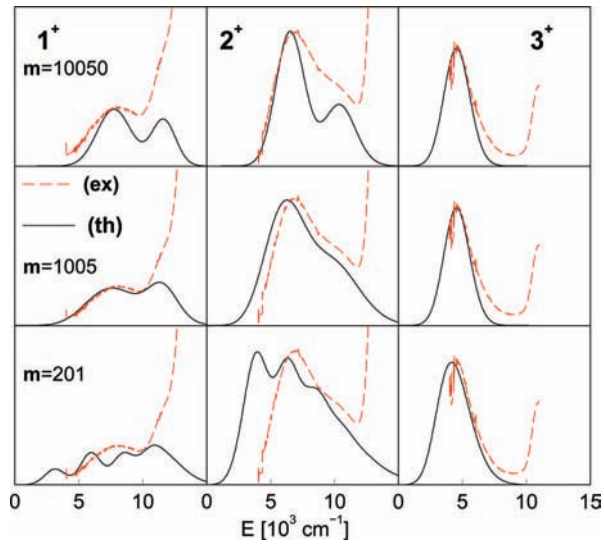

Figure 5. The influence of vibrational motion on absorption spectra of the systems $\mathbf{n}^+$. Calculated spectra (solid lines) are displayed for different mass parameters, as indicated. Also shown are measured spectra as dashed lines.

In the actual calculation we employed a large but finite value of $m = 10500$ because otherwise the ground-state vibrational wave function cannot be determined. It has to be noted that the adiabatic and diabatic Hamiltonians of eqs 7 and 10 are still not equivalent because the dipole matrix is treated as geometry independent. Naturally, different spectral features are to be expected which is demonstrated in Figure 4. There, the theoretically determined spectra σ_0^{d}, σ_0^{a} are shown for the three radical cations and for transitions out of the vibrational ground state ($i = 0$). In calculating the spectra, a Gaussian window function $w(t)$ is employed which leads to a spectral resolution of 1620 cm^{-1}. From the figure it is obvious, that differences exist which are largest for system $\mathbf{1}^+$ (upper panel). There, two bands are found which agree in position but differ in intensity. In the other two systems, the deviations are minor, being smallest in the case of the $\mathbf{3}^+$ system having only a single band (due to the fact that the dipole moment is nonzero only for the $|1> \rightarrow |2>$ transition, see, however, the discussion below). The deviations stem from the different coupling elements contained in the adiabatic/diabatic Hamiltonians. An analysis for the case where the deviations are largest (the $\mathbf{1}^+$ system) shows that the main reason for the disagreement between the calculated spectra is the Condon approximation for the dipole moment matrix. If, in going from the diabatic to the adiabatic representation (i.e., transforming $\mathbf{H}^{\mathrm{d}}$ (eq 7) into $\mathbf{H}^{\mathrm{a}}$ (eq 10)), this matrix is transformed employing the coordinate-dependent transformation matrix, both calculations give almost identical results. The fact that then the spectra are still not identical is due to the omission of kinetic couplings which arise upon transforming the kinetic energy operators in the Hamiltonian.

From the formulation given in the last section, it is already clear that the adiabatic approach allows for a simpler analysis of the spectral properties. First, the spectrum can be deconvoluted into a sum of single spectra (see eq 15), and second, neglecting the kinetic energy operator allows the establishment of a relation between the spectrum, the potential surfaces, and the initial vibrational wave function. This connection is commonly named the "reflection principle".[31] The intensity of the various bands (corresponding to transitions into distinct higher electronic states) directly scales with the square of the transition dipole moment μ_{1n}^{a} which can be seen in comparing Figure 4 with the values in Table 1. Thus, in what follows, we concentrate on the spectra resulting from the adiabatic description.

To investigate the influence of the internal vibrational motion on the optical properties, spectra are calculated for different values of the mass parameter m entering into the kinetic energy operators. The variation of m influences both the ground- and excited-state dynamics. In the ground state, the zero-point energy rises with decreasing mass which is accompanied by a more delocalized vibrational wave function. This is similar in the excited state where, because of the increasing level spacing, a vibrational progression can eventually be observed in the spectrum; see below.

Results for all radical cations and for three values of the mass parameter are displayed in Figure 5 which also contains the measured curves, for comparison. Note, that in the latter spectra there exist additional absorption bands at larger photon energies. These bands result from transitions to higher excited states which are not incorporated in our model.

Let us regard the $\mathbf{1}^+$ case as a first example. In lowering the value of the mass parameter to a value of $m = 1005$, the mere effect is that the two electronic bands are broadened so that the minimum around 10000 cm^{-1} becomes less pronounced. If the mass parameter is set to its smallest value $m = 201$, a clearer deviation occurs. First, absorption sets in at lower photon energies. Within a one-dimensional harmonic picture, the difference in zero-point energy in the excited and ground state is

$$\Delta E_0 = \Delta + \frac{1}{2\sqrt{m}}\left(\sqrt{k_2} - \sqrt{k_1}\right) \tag{19}$$

where Δ is the energy shift and k_n are the respective force constants. This means that the red shift occurring with decreasing mass is associated with a force constant being larger in the ground than in the excited state. Second, a vibrational structure becomes visible which is superimposed on the band splitting. These trends are also found for the $\mathbf{2}^+$ radical cation: with decreasing mass the two distinct electronic bands become less distinguishable. Furthermore a vibrational substructure and a red shift arises. On the other hand, the system $\mathbf{3}^+$ is less sensitive to the introduction of the kinetic energy. This essential difference between the $\mathbf{3}^+$ system and the others can be understood in

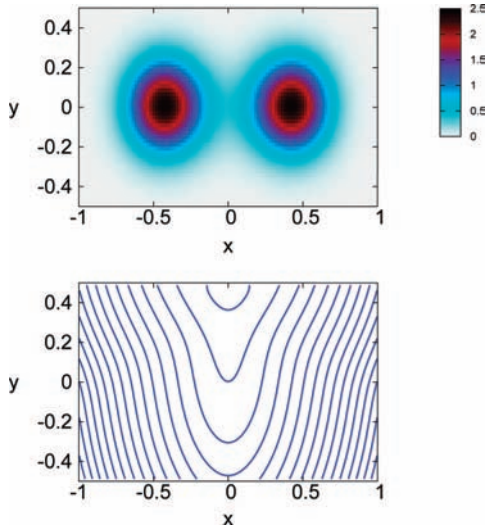

Figure 6. Adiabatic ground-state wave function (upper panel) and potential (lower panel) of the first excited state for the $\mathbf{2}^+$ system. The contours start at a value of 1000 cm^{-1} and increase in increments of 1000 cm^{-1}.

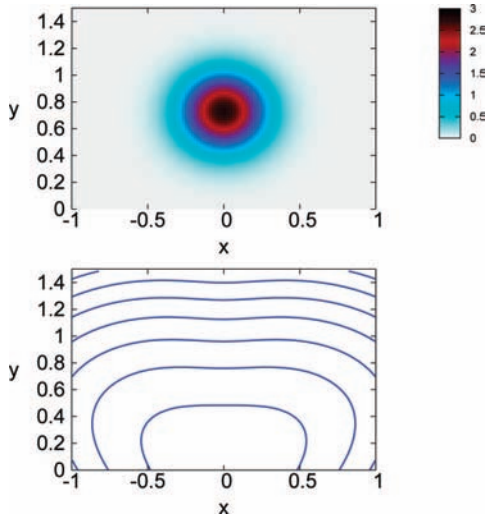

Figure 7. Same as Figure 6 but for the $\mathbf{3}^+$ system.

regarding the ground-state wave functions and excited-state potentials. In Figures 6 and 7, we show these functions for the $\mathbf{2}^+$ and $\mathbf{3}^+$ system, respectively. As already mentioned in the introduction, a double minimum structure is found in the potential energy surface of the $\mathbf{2}^+$system (this is similar in the case of $\mathbf{1}^+$, not shown) where the minima are deep enough to support a bound state. This corresponds to the situation where the hole is located at one of the two triarylamine groups. In a symmetry broken state then, there is density only on one of these groups. The vertical transition to the higher state has a Franck−Condon window which is well separated from the potential minimum and is localized in a region where the potential gradient is rather steep. Thus, a vibrational progression is to be expected. On the other hand, for the $\mathbf{3}^+$ system, the ground-state density is located at the bridge and a vertical transition ends up in a region where the excited-state potential has a small gradient. This means that the density of vibrational states is large and a much higher resolution is needed to observe a vibrational fine structure.

The role of the spectral resolution is illustrated in Figure 8 for the $\mathbf{1}^+$ system (and a mass parameter of $m = 1005$). In increasing the resolution from 1528 to 952 cm^{-1}, a vibrational substructure appears in the first absorption band. The peaks

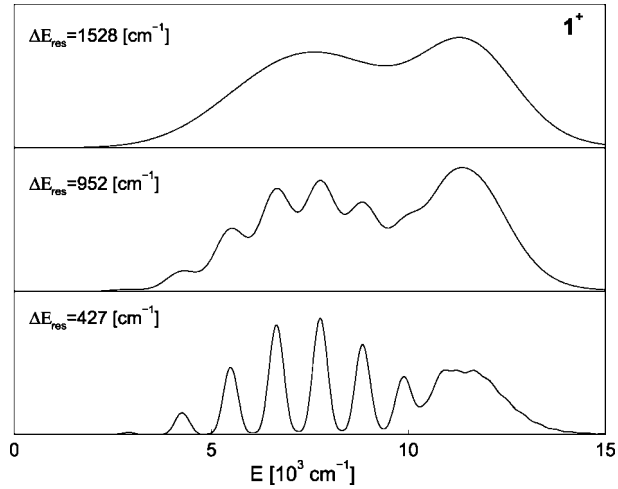

Figure 8. Adiabatically calculated absorption spectra for the $\mathbf{1}^+$ system employing different spectral resolutions ΔE_{res}, as indicated.

become sharper for an even higher resolution of 427 cm^{-1}. The vibrational spacing is found to be in the order of 1100 cm^{-1}. There is a diffuse structure on the second absorption band which shows that the resolution is still not large enough to resolve the respective vibrational structure corresponding to a smaller vibrational spacing (due to the shallow potential energy surface) in the second excited state.

We now turn to a comparison with experiment. For a given spectral resolution of $\Delta E = 1895$ cm^{-1} and a choice of the mass parameter of $m = 1005$, an excellent agreement with experiment is found for the systems $\mathbf{1}^+$ and $\mathbf{2}^+$; see Figure 5. As was already mentioned above, the strong absorption bands at energies larger than 13000 cm^{-1} are not described within our employed model. In the $\mathbf{2}^+$ case, the calculated spectrum is slightly red-shifted which suggests that a fine-tuning of the model parameters is appropriate (here, the red shift can easily be obtained by an energy shift of the adiabatic potential $V_2(x,y)$). This, however, is not within the scope of this work. The Gaussian-like absorption band for the $\mathbf{3}^+$ radical cation is also excellently reproduced for the choice of $m = 1005$ (where here a larger mass does not change the spectrum).

As was noted above, the relative intensity of the two absorption bands can be adjusted choosing different values for the adiabatic transition dipole moments. This trend is illustrated in regarding system $\mathbf{3}^+$. There is evidence for a small absorption band at higher energies[13] which is somehow hidden under the more intense single band with its center between 4000 and 5000 cm^{-1}. The additional band is easily obtained theoretically if the dipole moment $\mu_{13}{}^a$ is set to values different from zero. In Figure 9, lower panel, the spectra $\sigma_{0n}{}^a$ corresponding to the transitions into the excited states with $n = 2, 3$ are shown ($m = 10050$). They were normalized such that their maxima are of equal height. The sum of these spectra, calculated for two different ratios of the transition dipole moments $r_\mu = (\mu_{12}{}^a/\mu_{13}{}^a)$, are compared to experiment in the middle and upper panels. As expected, the addition of the high-energy spectral component yields to an enhanced total spectrum which is in excellent agreement with experiment for the ratio of $r_\mu = 2.14$. We thus conclude that, besides the simplicity of the reduced dimensionality model employed, there are still different parameter sets leading to very similar results and thus to a good agreement between theory and experiment.

Let us now compare the results of the quantum calculation to the classical determination of the absorption spectra as

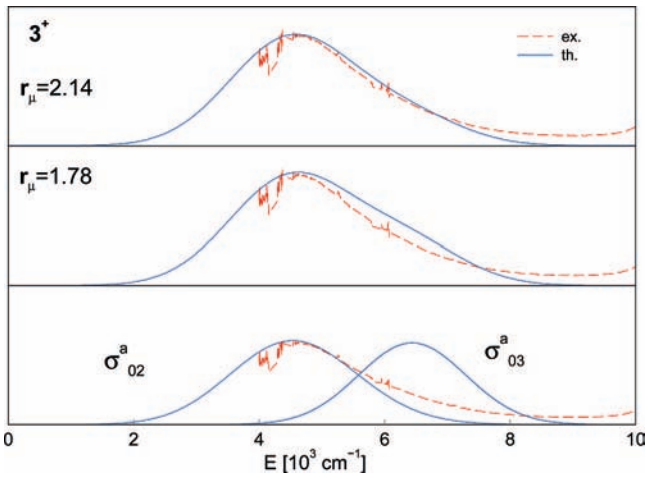

Figure 9. Comparison of calculated and measured absorption spectrum for the $\mathbf{3}^+$ system. The lower panel contains the partial spectra $\sigma_{0n}{}^a$ for the transition into the excited states $n = 2$ and 3, where the spectra are normalized to the same value at their respective maxima. The middle and upper panel contain the sum of the spectra for different ratios $r_\mu = \mu_{12}{}^a/\mu_{13}{}^a$ of the two transition dipole moments, as indicated.

detailed in ref 13. There, the adiabatic potentials were used to determine the spectra employing a Boltzmann distribution for the ground state and mapping this distribution via the difference potentials on the energy scale. This is close but not identical to our case of large mass ($m = 10050$), where the initial Boltzmann distribution is replaced by the quantum mechanical ground-state wave function. It is then not surprising that similar results are obtained which justifies our more simple approach taken before. One might then argue that the latter classical approach yields a good first description of the optical properties of the radical cations investigated here.

4. Summary

We present calculations on the absorption properties of three mixed valence systems. The theoretical model rests on the application of generalized Mulliken−Hush theory which yields model Hamiltonians expressed in a representation with potential (diabatic) or transition dipole (adiabatic) coupling elements. In a step further, vibrational motion is included in the Hamiltonians. Absorption spectra are calculated for various mass parameters which influences the time scale of the internal vibrational dynamics (and/or the vibrational level spacing). Depending on the system, the spectra derived from the diabatic or adiabatic representation differ. For one system ($\mathbf{1}^+$) it is found that the deviation is rooted in the Condon approximation employed for the transition dipole moments. Concerning the interpretation of the spectral features, the adiabatic representation offers the most direct approach. As is well-known, the spectrum is the sum of bands corresponding to the various electronic transitions. It is then more facile to tune the model parameters to achieve agreement with experiment. In the present case where, for all radical cations, the spectra do not show any vibrational progression, the mere effect of a vibrational motion is a broadening of the bands. This broadening can, of course, also be due to the coupling to the surroundings, i.e., the solvent. This is illustrated by comparing calculations for different mass parameters and spectral resolutions. Within the present model, which was set up before based on experimental and quantum chemical investigations, it is shown that a mass parameter of $m = 1005\ \mathrm{eV}^{-1}$ leads to an excellent agreement with experiment for all three radical cations. This leads to a vibrational spacing (in the first excited state) in the order of 1100 cm^{-1}, which is not unreasonable in view of recent resonance Raman measurements on similar systems.[28] In the future it will be necessary to gain more insight into the internal dynamics to arrive at a realistic picture of the role of nuclear motion. Here, femto- and picosecond time-resolved experiments offer a valuable tool to monitor this dynamics in real time.

Acknowledgment. Financial support by the DFG within the Graduiertenkolleg 1221 is gratefully acknowledged.

References and Notes

(1) Barbara, P. F.; Meyer, T. J.; Ratner, M. A. *J. Phys. Chem.* **1996**, *100*, 13148.
(2) Bredas, J.-L.; Beljonne, D.; Coropceanu, V.; Cornil, J. *Chem. Rev.* **2004**, *104*, 4971.
(3) Adams, D. M.; Brus, L.; Chidsey, C. E. D.; Creager, S.; Creutz, C.; Kagan, C. R.; Kamat, P. V.; Lieberman, M.; Lindsay, S.; Marcus, R. A.; Metzger, R. M.; Michel-Beyerle, M. E.; Miller, J. R.; Newton, M. D.; Rolison, D. R.; Sankey, O.; Schanze, K. S.; Yardley, J.; Zhu, X. *J. Phys. Chem. B* **2003**, *107*, 6668.
(4) *Electron Transfer in Chemistry*; Balzani, V., Ed.; Wiley-VCH: Weinheim, 2001.
(5) Demadis, K. D.; Hartshorn, C. M.; Meyer, T. J. *Chem. Rev.* **2001**, *101*, 2655.
(6) Launay, J.-P. *Chem. Soc. Rev.* **2001**, *30*, 386.
(7) Brunschwig, B. S.; Creutz, C.; N.; Sutin, N. *Chem. Soc. Rev* **2002**, *31*, 68.
(8) Nelsen, S. F. *Chem. Eur. J.* **2000**, *6*, 581.
(9) Nelsen, S. F.; Tran, H. Q.; Nagy, M. A. *J. Am. Chem. Soc.* **1998**, *120*, 298.
(10) Lindeman, S. V.; Rosokha, S. V.; Sun, D. L.; Kochi, J. K. *J. Am. Chem. Soc.* **2002**, *124*, 843.
(11) Nelsen, S. F.; Konradsson, A. E.; Y.; Teki, Y. *J. Am. Chem. Soc.* **2006**, *128*, 2902.
(12) Lambert, C.; Nöll, G.; Schelter, J. *Nat. Mater.* **2002**, *1*, 69.
(13) Lambert, C.; Amthor, S.; Schelter, J. *J. Phys. Chem. A* **2004**, *108*, 6474.
(14) Launay, J.-P.; Coudret, C.; Hortholary, C. *J. Phys. Chem. B* **2007**, *111*, 6788.
(15) Ko, J.; Ondrechen, M. J. *J. Am. Chem. Soc.* **1985**, *107*, 6161.
(16) Root, L. R.; Ondrechen, M. J. *Chem. Phys. Lett.* **1982**, *93*, 421.
(17) Borshch, S. A.; Kotov, I. N.; Bersuker, I. B. *Chem. Phys. Lett.* **1982**, *89*, 381.
(18) Amthor, S. B. N.; Lambert, C. *Chem. Phys.* **2005**, *316*, 141.
(19) Hush, N. S., Ed. In *Mixed-Valence Compounds*; Brown D. B., Ed.; D. Reidel Publishing Company: Dordrecht, 1980.
(20) Hush, N. S. *Coord. Chem. Rev.* **1985**, *64*, 135.
(21) Newton, M. D. *Adv. Chem. Phys.* **1999**, *106*, 303.
(22) Newton, M. D. *Chem. Rev.* **1991**, *91*, 767.
(23) Cave, R. J.; Newton, M. D. *Chem. Phys. Lett.* **1996**, *249*, 15.
(24) Hupp, J. T.; Williams, R. D. *Acc. Chem. Res.* **2001**, *34*, 505.
(25) Williams, R. D.; Hupp, J. T.; Ramm, M. T.; Nelsen, S. F. *J. Phys. Chem. A* **1999**, *103*, 11172.
(26) Bailey, S. E.; Zink, J. I.; Nelsen, S. F. *J. Am. Chem. Soc.* **2003**, *125*, 5939.
(27) Lockard, J. V.; Zink, J. I.; Konradsson, A. E.; Weaver, M. N.; Nelsen, S. F. *J. Am. Chem. Soc.* **2003**, *125*, 13471.
(28) Szeghalmi, A. V.; Erdmann, M.; Engel, V.; Schmitt, M.; Amthor, S.; Kriegisch, V.; Nöll, G.; Stahl, R.; Lambert, C.; Leusser, D.; Stalke, D.; Zabel, M. *J. Am. Chem. Soc.* **2004**, *126*, 7834.
(29) Gordon, R. G. *Adv. Magn. Reson.* **1968**, *3*, 1.
(30) Heller, E. J. *Acc. Chem. Res.* **1981**, *14*, 368.
(31) Schinke, R. *Photodissociation Dynamics*; Cambridge University Press: Cambridge, 1993.
(32) Tannor, D. J. *Introduction to Quantum Mechanics: A Time-dependent Perspective*; University Science Books: Sausalito, CA, 2007.
(33) Engel, V.; Schinke, R.; Hennig, S.; Metiu, H. *J. Chem. Phys.* **1990**, *92*, 1.
(34) Lockard, J. V.; Valverde, G.; Neuhauser, D.; Zink, J. I.; Luo, Y.; Weaver, M. N.; Nelsen, S. F. *J. Phys. Chem. A* **2006**, *110*, 57.
(35) Feit, M. D.; Fleck, J. A.; Steiger, A. *J. Comput. Phys.* **1982**, *47*, 412.
(36) Alvarellos, J.; Metiu, H. *J. Chem. Phys.* **1988**, *88*, 4957.
(37) Kosloff, R.; Tal-Ezer, H. *Chem. Phys. Lett.* **1986**, *127*, 223.

JP804779S